AGU ADVANCING EARTH AND SPACE SCIENCES

Geophysical Research Letters

RESEARCH LETTER
10.1029/2025GL120781

An Arctic Sea Ice Energy Budget for the Last Interglacial

M. Pollock[1], R. Diamond[2], H. Heorton[1], L. C. Sime[2], D. Schroeder[3], and C. Brierley[1]

[1]University College London, London, UK, [2]British Antarctic Survey, Cambridge, UK, [3]CPOM, University of Reading, Reading, UK

Key Points:

- Orbital differences led to increased incoming shortwave radiation during Arctic summers of the Last Interglacial compared to pre-industrial
- Consequent summer sea-ice loss differs widely between models and is strongly linked to shortwave energy anomalies at the surface
- The albedo feedback creates larger energy anomalies than the insolation changes and both warm the ocean surface to delay autumn freezing

Supporting Information:

Supporting Information may be found in the online version of this article.

Correspondence to:

M. Pollock,
matthew.pollock.23@ucl.ac.uk

Citation:

Pollock, M., Diamond, R., Heorton, H., Sime, L. C., Schroeder, D., & Brierley, C. (2026). An Arctic sea ice energy budget for the Last Interglacial. *Geophysical Research Letters*, *53*, e2025GL120781. https://doi.org/10.1029/2025GL120781

Received 25 NOV 2025
Accepted 27 FEB 2026

Author Contributions:

Formal analysis: M. Pollock
Investigation: M. Pollock
Methodology: M. Pollock, R. Diamond, H. Heorton, L. C. Sime, D. Schroeder, C. Brierley
Project administration: L. C. Sime, D. Schroeder, C. Brierley
Software: M. Pollock
Supervision: R. Diamond, H. Heorton, L. C. Sime, D. Schroeder, C. Brierley
Validation: M. Pollock
Visualization: M. Pollock
Writing – original draft: M. Pollock
Writing – review & editing: R. Diamond, H. Heorton, L. C. Sime, D. Schroeder, C. Brierley

Abstract With ongoing anthropogenic warming, the Arctic is increasingly dominated by thin, first-year sea ice. Understanding the ice–ocean–atmosphere interactions in warmer climates is therefore essential. We analyze the Arctic sea-ice energy budget in nine CMIP6-PMIP4 *lig127k* simulations of the Last Interglacial warm Arctic. All models show reduced Last Interglacial summer sea ice, but with substantial inter-model spread. We demonstrate that this arises from differences in surface energy anomalies, which are highly correlated with sea ice area anomalies (r^2 of 74%). Ice–albedo feedbacks dominate this response: reduced ice cover exposes more open ocean, enhances shortwave absorption, and warms the upper ocean. This heat is released in autumn, delaying sea-ice regrowth. Although modern warming is driven by longwave forcing, our results highlight that shortwave absorption from reduced albedo is a key driver of summer sea-ice loss, underscoring the need for accurate representation of surface heat-balance processes in future Arctic projections.

Plain Language Summary As the Earth warms, the Arctic Ocean is expected to be dominated by thin ice that forms and melts each year, with little thick multiyear ice. To understand the Arctic response under such conditions, we study the Last Interglacial period, 127,000 years ago, when changes in Earth's orbit caused the Arctic to receive more sunlight in spring and summer. Using nine state-of-the-art climate models, we investigate how energy moved between the atmosphere, ocean, and sea ice during this period, compared with pre-industrial conditions. We examine how much energy reached the surface, how much was reflected or absorbed, and how this energy was stored in the ocean. We find that differences in summer sea-ice cover between models are mainly driven by how much of the additional sunlight reaches the surface, and how much melting the ice changes the proportion that is reflected. Some extra energy is absorbed by the ocean, and later released in autumn. This delays regrowth, though winter ice area eventually returns. Although today's Arctic warming is driven mostly by greenhouse gases, our results show that accurately representing surface energy processes is essential for predicting how quickly summer sea ice will disappear in a warmer future.

1. Introduction

The seasonal melt and regrowth of sea ice, exposing and covering the dark open ocean surface, is the largest natural change in surface reflectivity on the planet (Perovich & Polashenski, 2012). The high albedo of Arctic sea ice thus strongly influences the global energy balance, with worldwide climate implications (Duspayev et al., 2024; IPCC, 2022). Sea-ice loss is a contributor to Arctic amplification, with the Arctic warming at nearly four times the global average (Rantanen et al., 2022). Ongoing anthropogenic warming is projected to drive the Arctic to ice-free summers, likely before mid-century (IPCC, 2019). As a result, summer Arctic sea ice may be the first major ecosystem to disappear due to climate change (Malhi et al., 2020).

Understanding the processes that govern the growth and melt of Arctic sea ice is critical. However, the system is highly non-linear, involving numerous positive and negative feedbacks (Serreze & Barry, 2011). While direct observations are challenging in such a remote and extreme environment (Perovich et al., 1999), climate models offer an opportunity to analyze sea-ice feedbacks (Notz & SIMIP, 2020). Co-ordinated multi-model efforts within the Coupled Model Intercomparison Project (CMIP) allow robust cross-comparison of sea ice and climate system responses across simulations (Eyring et al., 2016; Sime et al., 2025). The Last Interglacial (LIG; 130,000–116,000 years ago) is particularly useful for understanding sea-ice physics during warm conditions, as increased northern hemisphere spring insolation resulted in a warm Arctic (Kageyama et al., 2021; Otto-Bliesner et al., 2021; Sime et al., 2025). Proxy records suggest the Arctic was nearly sea-ice-free in summer (Guarino et al., 2020; Sime et al., 2023; Vermassen et al., 2023). Studying the LIG therefore allows us to investigate the climate dynamics of the Arctic under the warmer conditions of thin, first-year ice; conditions that are rapidly re-emerging today (Diamond et al., 2024; Kwok et al., 2020).

Within CMIP, the Last Interglacial was first represented by the PMIP4 *lig127k* experiment (Otto-Bliesner et al., 2017). This provides a co-ordinated multi-model ensemble with which to analyze how the orbitally driven insolation changes of the LIG impacted the Arctic sea-ice response. Alongside the direct impact of radiative anomalies, ocean temperatures play a substantial role in governing sea-ice thermodynamics. Large amounts of heat can be stored in the upper ocean, and thermal inertia impacts the timing of heat release (Lin et al., 2022; Ricker et al., 2021). Together, these factors underscore the importance of coupled surface heat exchanges in shaping the Arctic sea-ice response.

Previous work by Kageyama et al. (2021) studied an ensemble of models to assess sea-ice conditions in the Last Interglacial. However, at the time, data for a surface heat budget were limited to three models, and only net short- and longwave radiation was considered. Other studies have quantified heat budgets—including oceanic and atmospheric components—for individual models, for example, IPSL-CM6A-LR (Sicard et al., 2022); or shown the importance of model physics for determining the surface heat budget, for example, prognostic melt pond parameterizations in HadGEM3-GC3.1-LL (Diamond et al., 2024). These thermodynamic effects subsequently impact sea-ice melt and growth throughout the year (Keen et al., 2021). However, models show a wide range of variation in their sea-ice characteristics, both for future projections and paleoclimates (Kageyama et al., 2021; Notz & SIMIP, 2020; Notz et al., 2016). Robust conclusions independent of individual model behavior therefore require an analysis of model ensembles (Holland & Hunke, 2022). Here, we analyze an ensemble comprising the majority of models that simulated *lig127k*, including the models referred to above. We establish anomalies in the energy budget that includes both surface radiative and ocean mixed-layer heat components, and the resultant sea ice response. In a novel approach for the Last Interglacial, we also calculate the latent heat required to explain the anomalies in sea ice melt and growth. This allows us to identify causal links between sea-ice evolution and energy exchange processes across models that share identical boundary conditions, but differ in their physical parameterizations and resulting heat budgets.

2. Method

This study uses a multi-model ensemble of CMIP6–PMIP4 simulations to quantify how changes in surface radiation, ocean heat storage, and sea-ice processes together determine the Arctic sea-ice energy budget during the Last Interglacial, relative to pre-industrial conditions. Anomalies in seasonal climatologies, expressed as *lig127k*–*piControl*, are used to isolate the forced Last Interglacial response from mean-state variability. When Multi-Model Mean (MMM) results are quoted, the ensemble range (min-max) is indicated in square brackets.

The *piControl* simulations were run as part of CMIP6 (Eyring et al., 2016). These simulations use invariant solar, greenhouse gases, ozone, tropospheric aerosol, volcanic, and land-use forcing for the year 1850 and are spun up for several hundred years to attain a steady state. The *lig127k* simulations fully comply with the standard CMIP6-PMIP4 experimental protocol for LIG climate simulations, as described by Otto-Bliesner et al. (2017). The *lig127k* simulations were forced using constant 127k astronomical parameters (Berger & Loutre, 1991), and constant atmospheric trace GHG concentrations derived from ice core records (Otto-Bliesner et al., 2017). All other boundary conditions, including ice sheets, topography, vegetation, aerosol, volcanic activity, and solar constant, are identical to *piControl*.

Data were obtained from nine General Circulation Models (GCMs), where all necessary radiation and sea-ice outputs for both *lig127k* and *piControl* were available from the Earth System Grid Federation (Cinquini et al., 2014; https://esgf.github.io/nodes.html). An overview of the models is shown in Supporting Information S1 and further details can be found in Kageyama et al. (2021). Each model uses a variation of one of the sea-ice components: five models for CICE (Hunke et al., 2025); three models for LIM3 (Rousset et al., 2015); one model for COCO4, a combined ocean/sea-ice component model (Hasumi, 2006). In all cases, the region of interest was set to latitudes 60°N and higher, with a land mask applied. The orbital changes during the LIG mean that a fixed-angle calendar results in months of differing lengths compared with the pre-industrial (Bartlein & Shafer, 2019; Joussaume & Braconnot, 1997). However, available data are in standard-CMIP fixed-months, so adjustment to a fixed-angle would introduce incorrect lengths for melt and growth seasons, and associated energy budget calculations. Therefore, we follow the convention of not applying a paleo-calendar adjustment for an energy budget analysis (Otto-Bliesner et al., 2017; Pedersen et al., 2017).

2.1. Sea Ice Energy Budget

This study initially follows the approach that Kageyama et al. (2021) applied to three models, by quantifying the heat fluxes between the atmosphere and the ocean or sea-ice surface. For all flux calculations, we define positive values to indicate increasing energy into the Earth's surface. From the canonical equation of Maykut and Untersteiner (1971):

$$Q_{\text{atmos}} = (S_{\downarrow} - S_{\uparrow}) + (L_{\downarrow} - L_{\uparrow}) - \Theta_{\uparrow} \tag{1}$$

where Q_{atmos} is the net atmospheric heat flux (Wm^{-2}), $S_{\downarrow}$ is the downwelling shortwave radiative flux (Wm^{-2}), $S_{\uparrow}$ is the upwelling shortwave radiative flux (Wm^{-2}), $L_{\downarrow}$ is the downwelling longwave radiative flux (Wm^{-2}), $L_{\uparrow}$ is the upwelling longwave radiative flux (Wm^{-2}), and $\Theta_{\uparrow}$ is the net turbulent (sensible + latent) heat flux (Wm^{-2}).

In terms of the GCMs, standardized CMOR output (Balaji et al., 2018; Doutriaux et al., 2025), the equivalent terms are:

$$Q_{\text{atmos}} = (\text{rsds} - \text{rsus}) + (\text{rlds} - \text{rlus}) - (\text{hfss} + \text{hfls}) \tag{2}$$

$S_{\downarrow}$ represents the incoming insolation, modulated by shortwave absorption in the atmosphere. $S_{\uparrow}$ represents reflected shortwave radiation, controlled by the surface albedo. $\Theta_{\uparrow}$ relates to the transfer of heat from the surface to the atmosphere, including via state changes such as sublimation (Hunke et al., 2025; Maykut & Untersteiner, 1971). For each model, monthly data were available and a mean seasonal climatology of the terms in Equation 1 was calculated from the full production run. To understand the impact of anomalies in these terms, they were compared to anomalies in the energy required to melt or grow the sea ice each month, due to the latent heat of fusion. We define this quantity as Λ_{ice}. Note that Λ_{ice} is a change in the internal store of heat within sea ice, and should not be confused with the latent heat component in $\Theta_{\uparrow}$, which represents a flux between the ice and the atmosphere. Λ_{ice} is not a model output, and so was calculated from the change in sea-ice volume over each month (derived from sea-ice concentration, **siconc**, and thickness, **sithick**) and the bulk physical properties of sea ice: a latent heat of fusion set to $\lambda_{ice} = 3.34 \times 10^5$ Jkg^{-1}, and density of $\rho_{ice} = 917$ kgm^{-3}, in line with the sea-ice model components (Hunke et al., 2025). Finally, Λ_{ice} is scaled by total area and time per month to be presented in Wm^{-2}, and thus comparable to the fluxes in Equation 1. Therefore, for a given month:

$$\Lambda_{\text{ice}} = \frac{\Delta SIV \times \rho_{\text{ice}} \times \lambda_{\text{ice}}}{A \times t} \tag{3}$$

where Λ_{ice} is the energy required for a change in sea-ice volume due to the latent heat of fusion (Wm^{-2}); ΔSIV is the monthly change in sea-ice volume (m^3); ρ_{ice} is the density of sea ice (917 kgm^{-3}); λ_{ice} is the latent heat of fusion of sea ice (3.34×10^5 Jkg^{-1}); A is the total area over which ΔSIV is calculated (m^2); and t is the time in seconds in the month for which ΔSIV is calculated (s).

Closing the surface energy budget would require the oceanic heat flux and the conductive heat flux of the ice: F_O and G, respectively, as per Maykut and Untersteiner (1971). However, these are not direct model outputs. Instead, we calculated mixed-layer heat content based on sea-surface temperature (SST) and mixed-layer depth (**tos** and **mlotst**, respectively), which were available for all models except HadGEM3-GC3.1-LL and MIROC-ES2L. Physical parameters were taken as constants in line with the ocean model components: seawater density of $\rho_{sw} = 1{,}025$ kgm^{-3} and seawater specific heat of $C_{sw} = 3{,}993$ $\text{Jkg}^{-1o}\text{C}^{-1}$ (Madec et al., 2024; Pemberton et al., 2017). Again, this was scaled to be in units of Wm^{-2}, so that:

$$H_{\text{mixed}} = \frac{\Delta T \times d \times \rho_{\text{sw}} \times C_{\text{sw}}}{t} \tag{4}$$

where H_{mixed} is the energy change in the mixed layer due to the specific heat capacity of seawater (W m^{-2}); ΔT is the monthly change in mixed-layer temperature (°C); d is the mixed-layer depth (m); ρ_{sw} is the density of seawater

($1{,}025\ \mathrm{kg\ m^{-3}}$); C_{sw} is the specific heat capacity of seawater ($3{,}993\ \mathrm{J\ kg^{-1}\ °C^{-1}}$); and t is the time in seconds in the month for which ΔT is calculated (s).

Note that we do not need to scale by area, since the mixed-layer depth, rather than volume, is used.

3. Results

3.1. Sea Ice Response

Summer sea ice was substantially reduced in the *lig127k* (Figure 1b) relative to *piControl*, despite a similar area during the winter (Figure 1a). The MMM *piControl* summer minimum sea ice area (SIA) is 5.68 $\mathrm{Mkm^2}$ [inter-model range: 4.04–8.52], while for the *lig127k* it is reduced to 2.06 $\mathrm{Mkm^2}$ [0.40–3.49]. However, this simulated *lig127k* MMM is still positively biased relative to proxy reconstructions that suggest near ice-free summers during the Last Interglacial (Sime et al., 2023; Vermassen et al., 2023). Only HadGEM3-GC3.1-LL is seasonally ice-free for the majority of its *lig127k* run, with 93% of years below the 1.0 $\mathrm{Mkm^2}$ threshold. EC-Earth3 and CESM2 are seasonally ice-free for a substantial portion of the run (39% and 19%, respectively). A further three models (IPSL-CM6A-LR, NESM3, and NorESM1-F) are ice-free for less than 10% of the run years. The final three models (ACCESS-ESM1-5, EC-Earth3-LR, and MIROC-ES2L) are never ice-free. While there are substantial summer *lig127k–piControl* sea ice reductions across all models, winter reductions are much smaller. Indeed, three models (MIROC-ES2L, NESM3, and NorESM1-F) show increased winter SIA (Figure 1c).

3.2. Surface Radiative Fluxes

During the Last Interglacial, differences in orbital parameters led to changes in the seasonal and spatial distribution of incoming solar energy. All models use identical Top of Atmosphere (TOA) insolation forcing per experiment (Eyring et al., 2016), with anomalies over the region of interest (≥60°N) peaking at 72 $\mathrm{Wm^{-2}}$ in June, and reaching a minimum of $-56\ \mathrm{Wm^{-2}}$ in September. However, model differences in atmospheric physics lead to differences in downwelling short- and longwave radiation at the surface (Smith et al., 2020), shown in Figure 2b. Shortwave anomalies dominate the surface heat budget during the melt season (Figure 2c); the magnitude of net longwave anomalies remains below 6.0 $\mathrm{Wm^{-2}}$ [5.2–9.4] for all months (not shown). While many factors including snowfall and ice age impact the albedo across the Arctic Ocean basin, the principal driver is the area of open ocean versus sea ice (Perovich & Polashenski, 2012). Hence the seasonality in SIA anomalies is closely related to the seasonality in albedo (Figure 2d). The MMM annual minimum albedo falls to 14.8% [10.20%–16.90%] in *lig127k*, approximately half of the minimum *piControl* albedo (26.4% [21.5%–38.5%]). As thin first-year ice regrows faster than thicker multiyear ice (Lin et al., 2022), winter SIA is similar between *lig127k* and *piControl*. Similarly, winter maximum albedo is relatively unchanged between *lig127k* and *piControl* (Figure 2d). A lower summer surface albedo means a higher fraction of the downwelling shortwave energy is absorbed by the surface (Calmer et al., 2023). Q_{atmos} thus peaks in June at 45.3 $\mathrm{Wm^{-2}}$ [31.6–64.3]. This is substantially greater, and 1 month later, than the insolation-driven shortwave downwelling anomaly. Similarly, this albedo response offsets the negative downwelling anomalies in autumn, so that Q_{atmos} anomalies only fall to $-21.1\ \mathrm{Wm^{-2}}$ [−11.6 to −29.9].

Three models have high Q_{atmos} peak anomalies compared to the MMM: EC-Earth3, EC-Earth3-LR, and HadGEM3-GC3.1-LL (Figure 2c). For both EC-Earth3 models, this is driven by a drop in albedo significantly larger than the MMM (Figure 2d), despite a downwelling shortwave, $S\downarrow$, anomaly that is below the MMM (Figure 2b). For HadGEM3-GC3.1-LL, both the downwelling and albedo anomalies are close to the MMM. Instead, the key factor is the timing of the albedo change (Figure 2d): spring/summer albedo reduction occurs very rapidly, due to the particular explicit melt pond scheme in the HadGEM3-GC3.1-LL sea ice model (Diamond et al., 2024; Guarino et al., 2020). This leads to the maximum albedo reduction occurring while the downwelling insolation anomaly is still near its peak, leading to a higher peak Q_{atmos}. By definition, the upwelling shortwave ($S\uparrow$; Equation 1) anomaly is closely linked to the albedo response. Across models, the average and spread of the albedo-driven anomaly of $S\uparrow$ is larger than the insolation driven anomaly, $S\downarrow$: MMM of 32.0 $\mathrm{Wm^{-2}}$ [11.9–68.0] and 28.7 $\mathrm{Wm^{-2}}$ [18.7–40.0], respectively.

We find a strong relationship (Figure 3) between peak Q_{atmos} anomaly (the maxima in Figure 2c) and annual minimum SIA anomaly (the minima in Figure 2a). The inter-model r^2 is 74% ($p = 0.0029$). Averaging the EC-

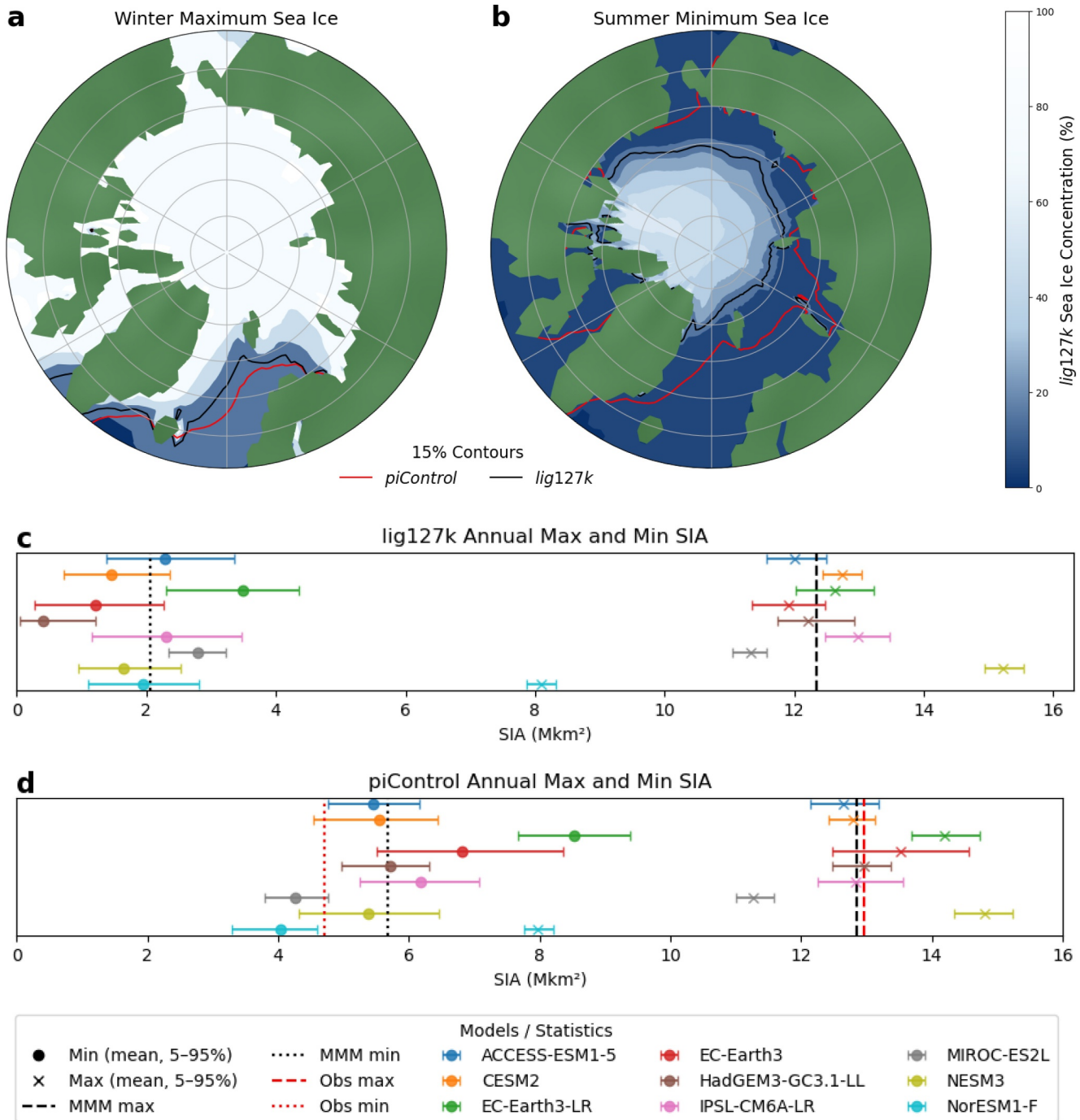

Figure 1. Winter maximum and summer minimum sea-ice area for *lig127k* and *piControl*. Panel (a) shows the multi-model mean (MMM) distribution of sea-ice concentration during the *lig127k* winter maximum, and the 15% concentration contours for the *lig127k* and *piControl*. Panel (b) shows the same for the summer minimum. Panel (c) shows the mean sea ice area (SIA) per model for the *lig127k*. Bars show the 5th-95th percentile of SIA from each model's full *lig127k* run. Vertical black dashed lines show the MMM. Panel (d) shows the same for the *piControl*, with observations shown as vertical red dashed lines. Observations are the average of the 10 years starting in 1979, from the National Snow and Ice Data Center (Fetterer et al., 2025).

Earth models to reduce data inter-dependency does not meaningfully change the result, $r^2 = 71\%$; $p = 0.0090$. The ice-albedo feedback means that the $S\uparrow$ component of Q_{atmos} is both a cause and response to reduced SIA (Perovich & Polashenski, 2012). However, we find the relationship between this component alone and minimum SIA anomalies to be weaker, at an r^2 of 49%. This suggests that including both the initial insolation anomaly and the

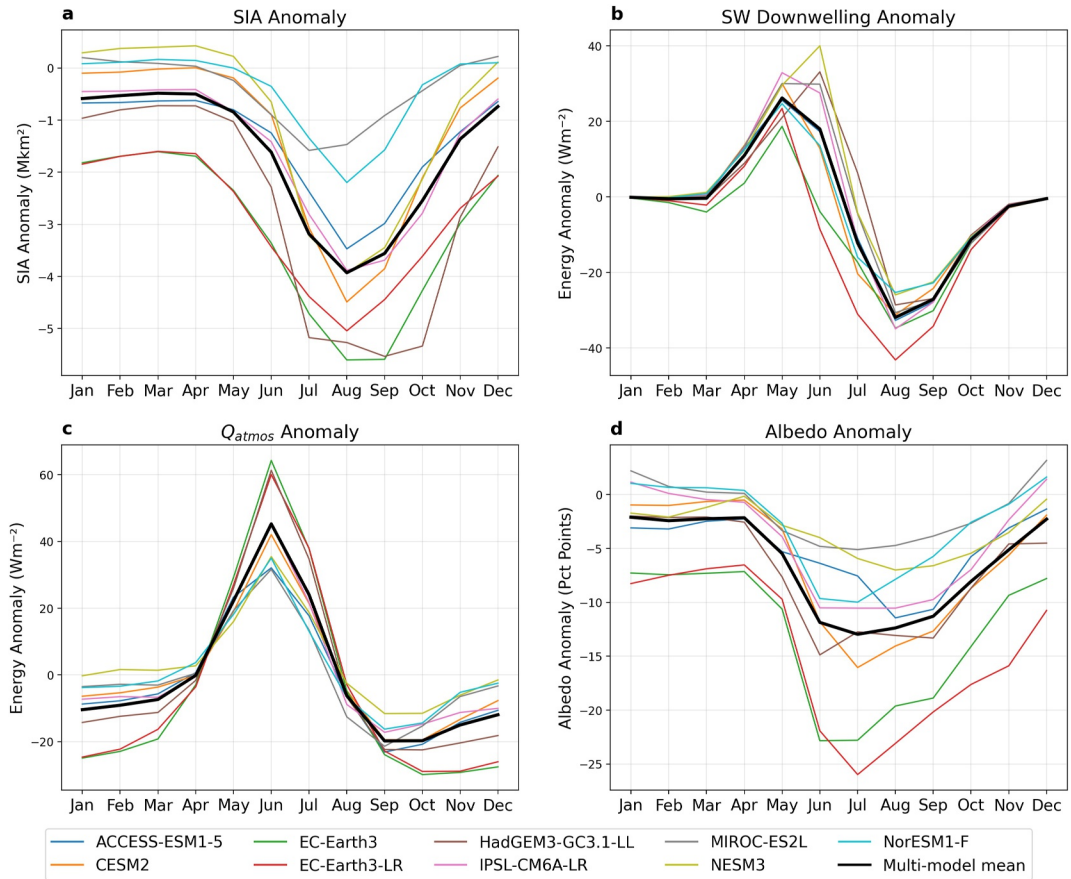

Figure 2. Seasonal climatologies of sea ice area (SIA) and radiative flux anomalies. Panel (a) shows the anomalies in SIA. Panel (b) shows the anomalies in downwelling shortwave radiation ($S\downarrow$) from insolation anomalies (attenuated by atmospheric processes). Panel (c) is the total heat flux, Q_{atmos}, anomaly (as defined in Equation 1). Panel (d) is the resultant anomaly in albedo across the Arctic Ocean basin.

albedo response is necessary in explaining sea-ice loss. Note that while the SIA anomaly is strongly correlated to the energy anomaly, it does not explain the absolute level of sea ice. EC-Earth-LR, for example, has a large SIA and Q_{atmos} anomaly but from a high pre-industrial baseline (Figure 1) and so is not ice-free (Figure 3).

3.3. The Ocean Mixed Layer

A greater expanse of (low albedo) open ocean during Last Interglacial spring and summers means that a portion of the Q_{atmos} anomalies acts to warm the ocean mixed layer (Dai et al., 2019). Full ocean temperature data were not readily available for the majority of the models, so a complete energy budget of the ocean is beyond the scope of this paper. However, we gain insight by comparing Q_{atmos} and Λ_{ice}, which we defined as the change in latent heat required to produce the anomalies in sea growth and melt (as detailed in the Method, Equation 3). The difference between the two is the energy available for exchange with the mixed layer of the ocean (Sicard et al., 2022), which we define as the *residual energy*.

A comparison between Q_{atmos} and Λ_{ice} (Figure 4) reveals that there are periods where radiative anomalies are well matched to the energy required for sea-ice latent heat anomalies (December–May); periods where there is additional radiative flux (June–August); and periods where radiative flux alone is insufficient to explain the change in growth/melt anomalies (September–November). From December to May, SIA anomalies remain small (Figure 2a), so downwelling shortwave radiation acts on the same area of open ocean in both the *lig127k* and *piControl*. Consequently, there is little residual energy anomaly: Q_{atmos} and Λ_{ice} are closely matched for December–May (Figure 4). Between June and August there is more open ocean (SIA anomalies become increasingly negative; Figure 2a). This allows for greater residual energy–shown by increasing differences

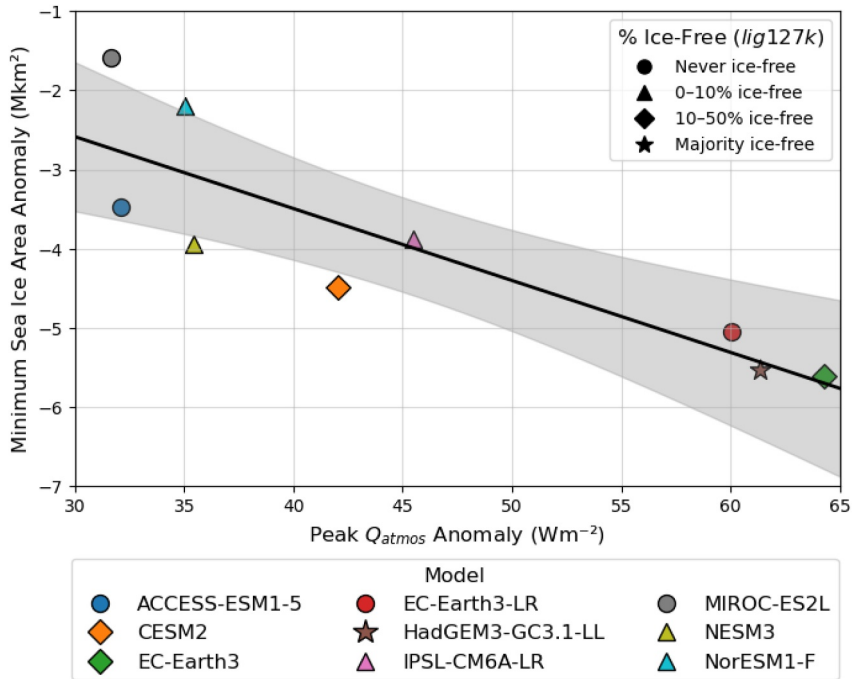

Figure 3. Linear regression over the peak total heat flux, Q_{atmos}, anomaly and the anomaly in the summer minimum sea ice area (SIA), per model. Marker shape indicates the proportion of the model run that is ice-free (percentage of model years with summer SIA below 1.0 Mkm^2). Gray shading is the 95% confidence interval of the regression. The r^2 is 74% ($p = 0.0029$).

between Q_{atmos} and Λ_{ice} in Figure 4–which warms the ocean surface. This leads to a strong relationship between anomalies in melt-season residual energy and peak SSTs, $r^2 = 81\%$ (Figure S1 in Supporting Information S1). The thermal inertia of the ocean (Markus et al., 2009) means this heat is slowly released between September and November, so the difference between Q_{atmos} and Λ_{ice} turns negative. While the SIA recovers faster during the LIG growth season–due to the negative insolation anomalies, and more rapid growth of thin first-year ice (Lin

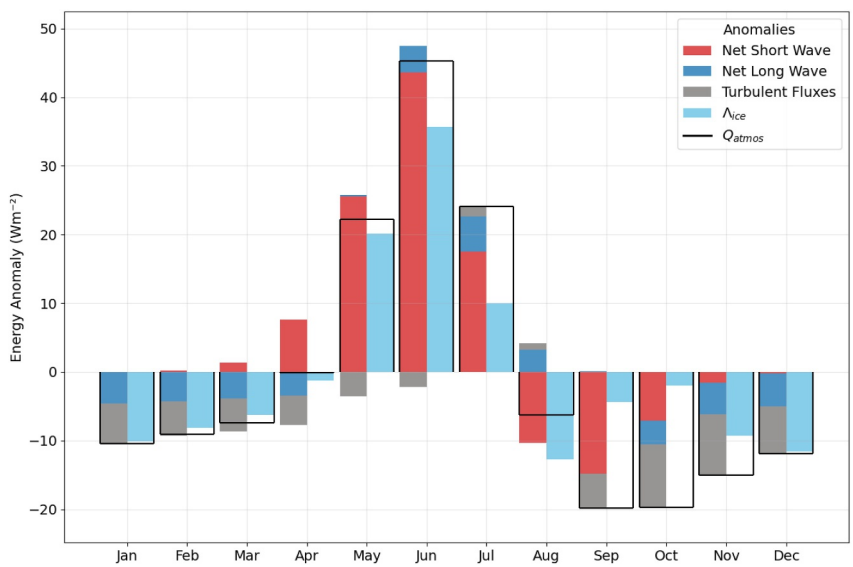

Figure 4. Comparison of radiative flux anomalies (stacked colored bars) versus energy calculated to explain the latent heat required for sea-ice volume anomalies, Λ_{ice} (light blue bars). Black lines are the total heat flux anomalies, Q_{atmos}, that is, the sum of shortwave, longwave, and turbulent flux anomalies. The difference between Q_{atmos} and Λ_{ice} represents radiative energy anomalies that are not directly leading to melt/growth anomalies.

et al., 2022)–release of ocean heat restricts the growth from September to November compared to growth expected from the anomalies in Q_{atmos} alone (Figure 4, months September–November). Growth, and SIA, subsequently recovers in the late winter and spring. SST anomalies reflect this seasonality, with MMM anomalies below 0.5°C [−0.25°C–0.85°C] from Jan to May, before warming to 2.5°C [1.22°C–4.66°C] in August, subsequently falling back below 0.5°C [−0.17°C–1.18°C] by November. Anomalies in ocean heat transport into the region of interest (≥60°N) were calculated for four models where data was available. These were either negative (EC-Earth3, IPSL-CM6A-LR) or small relative to Q_{atmos} (<7 Wm^{-2} equivalent annual average, EC-Earth3-LR, HadGEM3-GC3.1-LL), which reinforces the strong relationship between residual energy and SSTs shown in Figure S1 in Supporting Information S1.

However, the seasonality of SST anomalies alone is not well aligned with the residual energy as they do not take into account anomalies in the volume of water in the mixed layer. SST anomalies modulated by mixed-layer depth anomalies (Method, Equation 4) are a better proxy for specific heat (Patrizio & Thompson, 2021). During the *lig127k* there is earlier and greater shoaling of the mixed layer than the *piControl*, shown in Figure S2 in Supporting Information S1, due to the earlier and more extensive influx of fresh water from ice melt (Randelhoff et al., 2017). The magnitude of the specific heat anomalies calculated by Equation 4 matches the residual energy well during the period of mixed layer shoaling (Figure S3 in Supporting Information S1), as heat exchange between the mixed layer and the deeper ocean is limited (Cole & Roemer, 2024). There are larger discrepancies during the period of deepening of the mixed layer, as data for the temperature of the entrained water was not available for most models, and so excluded in this approach. However, the phasing remains aligned throughout the year reflecting the causal relationship between the two.

Lastly, we consider the final potential heat store within the surface energy budget and determine bounds for the average specific heat of the sea ice (Sicard et al., 2022). Details of the approach are in Supporting Information S1. Assuming a bulk sea-ice salinity of 2‰ in both experiments, 12.5 Wm^{-2} less radiation is required to heat the lower volume of *lig127k* ice compared to the *piControl*. However, the specific heat capacity of ice depends on its temperature and salinity; younger and consequently more saline ice has a higher specific heat capacity. Assuming 2‰ salinity in *piControl* and 5‰ for the younger *lig127k* ice (Griewank & Notz, 2015) yields an upper bound of 7.5 Wm^{-2} additional energy required to warm *lig127k* ice during melt season compared to *piControl*. In both cases anomalies during the growth season are small (Figure S4 in Supporting Information S1). Thus the potential impact is limited compared to other reservoirs of energy, but without sea-ice salinity and temperature tracers from the models, the exact scale and direction of impact cannot be verified.

4. Discussion and Conclusion

With ongoing global warming, the Arctic is transitioning from a region dominated by thick, multiyear ice to one characterized by thinner first-year ice, and substantially reduced summer ice cover (Granskog et al., 2018; Kacimi & Kwok, 2022). Given the complexity of sea-ice growth and melt (Keen et al., 2021), our current understanding of the region may become outdated as this progresses (Krumpen et al., 2025; Sumata et al., 2023). Previous studies have shown that CMIP6 models tend to overestimate sea ice in the LIG while more accurately representing the Pre-Industrial (Notz & SIMIP, 2020; Otto-Bliesner et al., 2021; Sime et al., 2023; Vermassen et al., 2023), which aligns with the ensemble used here (Figure 1). Our analysis shows that the correlation between surface energy anomalies and SIA anomalies remains high across a large range of energies. This study also highlights the importance of the ocean mixed layer as a store of heat in warmer climates, delaying winter freeze-up (Figure 4), a process which is known to be extending the melt season in the modern-day Arctic (Markus et al., 2009; Stroeve et al., 2014). The strong relationship between Q_{atmos} and the reduction in summer SIA (Figure 3) and between the residual energy and ocean warmth (Figure S1 in Supporting Information S1) highlight the importance of radiative energy in driving sea-ice loss through both direct and indirect means.

The importance of the albedo feedback during the LIG summer has been demonstrated previously for individual models (Diamond et al., 2024; Sicard et al., 2022). Here we show that, across a wide range of models, the *lig127k*–*piControl* anomalies in energy absorbed at the surface during the summer due to changes in albedo, $S\uparrow$, are larger than the anomalies due to the initial insolation differences, $S\downarrow$ (MMM of 32.0 Wm^{-2} and 28.7 Wm^{-2}, respectively). Through June-July-August, the diminishing sea-ice cover exposes more low-albedo open ocean, which takes up heat. This leads to increasing summer SST anomalies, accelerating the ongoing sea-ice melt. Models with higher residual energy show greater ocean surface warming (Figure S1 in Supporting Information S1). The

lig127k increase in mixed-layer heat content is partially compensated by earlier shoaling of the layer, due to earlier influx of freshwater from ice melt (Randelhoff et al., 2017), which reduces the total store of heat in the mixed layer. Nevertheless, the autumn growth is delayed as this heat is released (Markus et al., 2009; Stroeve et al., 2014). However, in *lig127k* the reduced growth season insolation (Figure 2b)–and the rapid growth of thin first-year sea ice (Lin et al., 2022)–outweighs the additional ocean heat release, allowing *lig127k* winter SIA to recover to near-*piControl* levels. Consequently, while the initial insolation anomalies are close to zero when averaged over the whole year, large negative SIA anomalies are seen in the summer (*piControl* SIA MMM of 5.68 Mkm^2 compared to 2.06 Mkm^2 for the *lig127k*) while winter SIA anomalies remain small.

There is a large spread in the net heat fluxes between the surface and the atmosphere, Q_{atmos} (Equation 1), across the models studied. The peak in Q_{atmos} ranges from 31.6 Wm^{-2} (MIROC-ES2L) to 64.3 Wm^{-2} (EC-Earth3). The *lig127k* summer SIA anomaly strongly depends on the Q_{atmos} peak (r^2 = 74%; Figure 3) indicating that inter-model differences in summer sea-ice loss are largely explained by the spread in the surface energy balance. Therefore, accurate simulation of sea ice requires accurate representation of the processes that influence Q_{atmos}. Cloud physics is a known source of large model discrepancy in the radiation reaching the surface (Arima et al., 2025; Kim et al., 2024; McCusker et al., 2023). Here we find that the surface radiation from insolation anomalies ranges by more than a factor of two, from 18.70 Wm^{-2} to 40.0 Wm^{-2} (EC-Earth3 and NESM3, respectively, Figure 2c), despite all models having the same TOA insolation. Consequently, cloud and aerosol feedbacks play a role in sea-ice characteristics by influencing the energy balance (Sicard et al., 2022; Smith et al., 2020). Similarly, $S\uparrow$ is the largest component of the anomalies in Q_{atmos}. The $S\uparrow$ term is closely linked to ice-albedo feedbacks, meaning the parametrization of sea-ice physics is an important factor determining sea-ice loss. While EC-Earth3, for example, has the lowest insolation anomaly at the surface, its highly sensitive albedo parametrization results in the highest Q_{atmos} energy anomaly, and consequently the greatest reduction in SIA of all the models studied (Figure 2). HadGEM3-GC3.1-LL highlights the importance of the timing, as well as the scale, of the albedo response. While the magnitude of the albedo reduction is close to the ensemble average, it occurs more rapidly due to the prognostic melt pond scheme, and thus peaks while the surface insolation anomaly is still high (Diamond et al., 2021). This leads to a higher peak in Q_{atmos} and consequently larger reduction in SIA.

While current and future Arctic sea-ice loss is principally caused by a year-round increase in longwave radiation from greenhouse gases (Docquier et al., 2024), rather than seasonal shortwave insolation changes, our study highlights the critical role of the surface energy balance in controlling summer sea-ice retreat. In particular, the enhanced spring and summer absorption of shortwave radiation due to reduced albedo not only has an immediate effect on sea ice, but influences ocean surface temperatures which subsequently delays autumnal growth. In *lig127k*, this delay occurs at a time of year when the insolation anomalies are negative (Figure 2b), a countering effect that is not present in the observed lengthening of the present-day melt season with potential implications for future winter sea-ice recovery (Stroeve et al., 2014). Variations in model physics that influence downwelling shortwave radiation at the surface, and the subsequent albedo response, will therefore contribute to variation in both the summer sea-ice loss, and the timing of the growth season. Understanding the behavior of sea ice in the Last Interglacial allows us to examine these mechanisms in a regime of thin, seasonal sea ice. By studying these processes in a past warm climate, we can better anticipate how similar feedbacks may amplify Arctic sea-ice loss under future warming.

Acronyms

TOA	Top of Atmosphere
SIA	Sea Ice Area
MMM	Multi-Model Mean
LIG	Last Interglacial
ESGF	Earth System Grid Federation
GCM	General Circulation Model
SST	Sea Surface Temperature

CMIP Coupled Model Intercomparison Project

Conflict of Interest

The authors declare no conflicts of interest relevant to this study.

Availability Statement

This research was undertaken using climate model output created for the Coupled Model Intercomparison Project. It is freely available for download via the Earth System Grid Federation (Cinquini et al., 2014; https://esgf-node.llnl.gov/search/cmip6/, last access: 18 June 2025). Unfortunately, output from the HadGEM3-GC31-LL *lig127k* experiment has not been lodged with the ESGF. The climatological fields and time-series data used within this research are available instead on Zenodo (doi: https://doi.org/10.5281/zenodo.17650994), which also contains the python code used to create the figures (Pollock, 2025).

Acknowledgments
This science would not be possible without the generous contributions of climate model experiments that have been performed in support of the Palaeoclimate Modelling Intercomparison Project. MP and RD acknowledge support from NERC training Grants NE/S007229/1 and NE/S007164/1, respectively. CB is supported through NE/Y001443/1. LCS is supported through: Past-to-Future: Towards fully paleo-informed future climate projections (P2F), GN 101184070; NERC-SWAIS2C, NE/X009386/1; and NERC-KANG-GLAC, NE/V006509/1. This work was supported by NERC through National Capability funding, undertaken by a partnership between the Centre for Polar Observation Modelling and the British Antarctic Survey.

References

Arima, N., Yoshimori, M., Abe-Ouchi, A., O'ishi, R., Chan, W.-L., Sherriff-Tadano, S., & Ogura, T. (2025). Impact of the temperature-cloud phase relationship on the simulated arctic warming during the last interglacial. *EGUsphere*, *2025*, 1–26. https://doi.org/10.5194/egusphere-2025-4109

Balaji, V., Taylor, K. E., Juckes, M., Lawrence, B. N., Durack, P. J., Lautenschlager, M., et al. (2018). Requirements for a global data infrastructure in support of CMIP6. *Geoscientific Model Development*, *11*(9), 3659–3680. https://doi.org/10.5194/gmd-11-3659-2018

Bartlein, P. J., & Shafer, S. L. (2019). Paleo calendar-effect adjustments in time-slice and transient climate-model simulations (PaleoCalAdjust v1.0): Impact and strategies for data analysis. *Geoscientific Model Development*, *12*(9), 3889–3913. https://doi.org/10.5194/gmd-12-3889-2019

Berger, A., & Loutre, M.-F. (1991). Insolation values for the climate of the last 10 million years. *Quaternary Science Reviews*, *10*(4), 297–317. https://doi.org/10.1016/0277-3791(91)90033-Q

Calmer, R., de Boer, G., Hamilton, J., Lawrence, D., Webster, M. A., Wright, N., et al. (2023). Relationships between summertime surface albedo and melt pond fraction in the central Arctic Ocean: The aggregate scale of albedo obtained on the MOSAiC floe. *Elementa*, *11*(1), 1575–1589. https://doi.org/10.1525/elementa.2023.00001

Cinquini, L., Crichton, D., Mattmann, C., Harney, J., Shipman, G., Wang, F., et al. (2014). The Earth System Grid Federation: An open infrastructure for access to distributed geospatial data. *Future Generation Computer Systems*, *36*, 400–417. https://doi.org/10.1016/j.future.2013.07.002

Cole, S. T., & Roemer, P. A. (2024). The transition layer and remnant transition layer of the western Arctic Ocean: Stratification, vertical diffusivity, and Pacific summer water heat fluxes. *Journal of Geophysical Research: Oceans*, *129*(2), e2023JC020059. https://doi.org/10.1029/2023JC020059

Dai, A., Luo, D., Song, M., & Liu, J. (2019). Arctic amplification is caused by sea-ice loss under increasing CO_2. *Nature Communications*, *10*(1), 121. https://doi.org/10.1038/s41467-018-07954-9

Diamond, R., Schroeder, D., Sime, L. C., Ridley, J., & Feltham, D. (2024). The significance of the melt-pond scheme in a CMIP6 global climate model. *Journal of Climate*, *37*(1), 249–268. https://doi.org/10.1175/JCLI-D-22-0902.1

Diamond, R., Sime, L. C., Schroeder, D., & Guarino, M. V. (2021). The contribution of melt ponds to enhanced Arctic sea-ice melt during the last interglacial. *The Cryosphere*, *15*(11), 5099–5114. https://doi.org/10.5194/tc-15-5099-2021

Docquier, D., Massonnet, F., Ragone, F., Sticker, A., Fichefet, T., & Vannitsem, S. (2024). Drivers of summer Arctic sea-ice extent at interannual time scale in CMIP6 large ensembles revealed by information flow. *Scientific Reports*, *14*(1), 24236. https://doi.org/10.1038/s41598-024-76056-y

Doutriaux, C., Taylor, K. E., Mauzey, C., Nadeau, D., & Durack, P. J. (2025). *The climate model output rewriter (CMOR3)*. Zenodo. https://doi.org/10.5281/zenodo.16760843

Duspayev, A., Flanner, M. G., & Riihelä, A. (2024). Earth's sea ice radiative effect from 1980 to 2023. *Geophysical Research Letters*, *51*(14), e2024GL109608. https://doi.org/10.1029/2024GL109608

Eyring, V., Bony, S., Meehl, G. A., Senior, C. A., Stevens, B., Stouffer, R. J., & Taylor, K. E. (2016). Overview of the coupled model intercomparison project phase 6 (CMIP6) experimental design and organization. *Geoscientific Model Development*, *9*(5), 1937–1958. https://doi.org/10.5194/gmd-9-1937-2016

Fetterer, F., Knowles, K., Meier, W. N., Savoie, M., Windnagel, A., & Stafford, T. (2025). *Sea ice index, version 4*. National Snow and Ice Data Center. https://doi.org/10.7265/A98X-0F50

Granskog, M. A., Fer, I., Rinke, A., & Steen, H. (2018). Atmosphere-ice-ocean-ecosystem processes in a thinner Arctic Sea ice regime: The Norwegian Young Sea ICE (N-ICE2015) expedition. *Journal of Geophysical Research: Oceans*, *123*(3), 1586–1594. https://doi.org/10.1002/2017JC013328

Griewank, P. J., & Notz, D. (2015). A 1-D modelling study of Arctic sea-ice salinity. *The Cryosphere*, *9*(1), 305–329. https://doi.org/10.5194/tc-9-305-2015

Guarino, M.-V., Sime, L. C., Schröeder, D., Malmierca-Vallet, I., Rosenblum, E., Ringer, M., et al. (2020). Sea-ice-free arctic during the last interglacial supports fast future loss. *Nature Climate Change*, *10*(10), 928–932. https://doi.org/10.1038/s41558-020-0865-2

Hasumi, H. (2006). *CCSR ocean component model (COCO) version 4.0* (Vol. 25, p. 103). Center for Climate System Research Report, Univ. of Tokyo.

Holland, M., & Hunke, E. (2022). A review of Arctic Sea ice climate predictability in large-scale Earth system models. *Oceanography*. https://doi.org/10.5670/oceanog.2022.113

Hunke, E., Allard, R., Bailey, D. A., Blain, P., Clemens-Sewall, D., Craig, A., et al. (2025). CICE-Consortium/CICE: CICE version 6.6.1. *Zenodo*. https://doi.org/10.5281/zenodo.16422732

IPCC. (2019). Chapter 3: Polar regions. In *IPCC special report on the ocean and cryosphere in a changing climate*. https://doi.org/10.1017/9781009157964.005

IPCC. (2022). *The ocean and cryosphere in a changing climate: Special report of the intergovernmental panel on climate change*. Cambridge University Press. https://doi.org/10.1017/9781009157964

Joussaume, S., & Braconnot, P. (1997). Sensitivity of paleoclimate simulation results to season definitions. *Journal of Geophysical Research*, *102*(D2), 1943–1956. https://doi.org/10.1029/96JD01989

Kacimi, S., & Kwok, R. (2022). Arctic snow depth, ice thickness, and volume from ICESat-2 and CryoSat-2: 2018–2021. *Geophysical Research Letters*, *49*(5), e2021GL097448. https://doi.org/10.1029/2021GL097448

Kageyama, M., Sime, L. C., Sicard, M., Guarino, M.-V., de Vernal, A., Stein, R., et al. (2021). A multi-model CMIP6-PMIP4 study of Arctic sea ice at 127 ka; sea ice data compilation and model differences. *Climate of the past*, *17*(1), 37–62. https://doi.org/10.5194/cp-17-37-2021

Keen, A., Blockley, E., Bailey, D. A., Boldingh Debernard, J., Bushuk, M., Delhaye, S., et al. (2021). An inter-comparison of the mass budget of the Arctic sea ice in CMIP6 models. *The Cryosphere*, *15*(2), 951–982. https://doi.org/10.5194/tc-15-951-2021

Kim, D., Kang, S. M., Kim, H., & Taylor, P. C. (2024). Quantifying changes in the Arctic shortwave cloud radiative effects. *Journal of Geophysical Research: Atmospheres*, *129*(15), e2023JD040707. https://doi.org/10.1029/2023JD040707

Krumpen, T., von Albedyll, L., Bünger, H. J., Castellani, G., Hartmann, J., Helm, V., et al. (2025). Smoother sea ice with fewer pressure ridges in a more dynamic Arctic. *Nature Climate Change*, *15*(1), 66–72. https://doi.org/10.1038/s41558-024-02199-5

Kwok, R., Kacimi, S., Webster, M., Kurtz, N., & Petty, A. (2020). Arctic snow depth and sea ice thickness from ICESat-2 and CryoSat-2 freeboards: A first examination. *Journal of Geophysical Research: Oceans*, *125*(3), e2019JC016008. https://doi.org/10.1029/2019JC016008

Lin, L., Lei, R., Hoppmann, M., Perovich, D. K., & He, H. (2022). Changes in the annual sea ice freeze–thaw cycle in the Arctic Ocean from 2001 to 2018. *The Cryosphere*, *16*(12), 4779–4796. https://doi.org/10.5194/tc-16-4779-2022

Madec, G., Bell, M., Benshila, R., Blaker, A., Boudrallé-Badie, R., Bricaud, C., et al. (2024). NEMO ocean engine reference manual. *NEMO Ocean Engine Reference Manual*. https://doi.org/10.5281/zenodo.14515373

Malhi, Y., Franklin, J., Seddon, N., Solan, M., Turner, M. G., Field, C. B., & Knowlton, N. (2020). Climate change and ecosystems: Threats, opportunities and solutions. *Philosophical Transactions of the Royal Society B: Biological Sciences*, *375*(1794), 20190104. https://doi.org/10.1098/rstb.2019.0104

Markus, T., Stroeve, J. C., & Miller, J. (2009). Recent changes in Arctic sea ice melt onset, freezeup, and melt season length. *Journal of Geophysical Research*, *114*(C12), C12024. https://doi.org/10.1029/2009JC005436

Maykut, G. A., & Untersteiner, N. (1971). Some results from a time-dependent thermodynamic model of sea ice. *Journal of Geophysical Research*, *76*(6), 1550–1575. https://doi.org/10.1029/JC076i006p01550

McCusker, G. Y., Vüllers, J., Achtert, P., Field, P., Day, J. J., Forbes, R., et al. (2023). Evaluating Arctic clouds modelled with the unified model and integrated forecasting system. *Atmospheric Chemistry and Physics*, *23*(8), 4819–4847. https://doi.org/10.5194/acp-23-4819-2023

Notz, D., Jahn, A., Holland, M., Hunke, E., Massonnet, F., Stroeve, J., et al. (2016). The CMIP6 sea-ice model intercomparison project (SIMIP): Understanding sea ice through climate-model simulations. *Geoscientific Model Development*, *9*(9), 3427–3446. https://doi.org/10.5194/gmd-9-3427-2016

Notz, D., & SIMIP. (2020). Arctic sea ice in CMIP6. *Geophysical Research Letters*, *47*(10), e2019GL086749. https://doi.org/10.1029/2019GL086749

Otto-Bliesner, B. L., Braconnot, P., Harrison, S. P., Lunt, D. J., Abe-Ouchi, A., Albani, S., et al. (2017). The PMIP4 contribution to CMIP6 – Part 2: Two interglacials, scientific objective and experimental design for Holocene and last interglacial simulations. *Geoscientific Model Development*, *10*(11), 3979–4003. https://doi.org/10.5194/gmd-10-3979-2017

Otto-Bliesner, B. L., Brady, E. C., Zhao, A., Brierley, C. M., Axford, Y., Capron, E., et al. (2021). Large-scale features of last interglacial climate: Results from evaluating the lig127k simulations for the coupled model intercomparison project (CMIP6)–paleoclimate modeling intercomparison project (PMIP4). *Climate of the Past*, *17*(1), 63–94. https://doi.org/10.5194/cp-17-63-2021

Patrizio, C. R., & Thompson, D. W. J. (2021). Quantifying the role of ocean dynamics in ocean mixed layer temperature variability. *Journal of Climate*, *34*(7), 2567–2589. https://doi.org/10.1175/JCLI-D-20-0476.1

Pedersen, R. A., Langen, P. L., & Vinther, B. M. (2017). The last interglacial climate: Comparing direct and indirect impacts of insolation changes. *Climate Dynamics*, *48*(9), 3391–3407. https://doi.org/10.1007/s00382-016-3274-5

Pemberton, P., Löptien, U., Hordoir, R., Höglund, A., Schimanke, S., Axell, L., & Haapala, J. (2017). Sea-ice evaluation of NEMO-Nordic 1.0: A NEMO-LIM3.6-based ocean-sea-ice model setup for the North Sea and Baltic Sea. *Geoscientific Model Development*, *10*(8), 3105–3123. https://doi.org/10.5194/gmd-10-3105-2017

Perovich, D. K., Andreas, E. L., Curry, J. A., Eiken, H., Fairall, C. W., Grenfell, T. C., et al. (1999). Year on ice gives climate insights. *Eos, Transactions American Geophysical Union*, *80*(41), 481–486. https://doi.org/10.1029/EO080i041p00481-01

Perovich, D. K., & Polashenski, C. (2012). Albedo evolution of seasonal Arctic sea ice. *Geophysical Research Letters*, *39*(8), L08501. https://doi.org/10.1029/2012GL051432

Pollock, M. (2025). *mattpollock100/CMIP6EnergyBudget: CMIP6 energy budget code and data (version CMIP6EnergyBudget) [Collection]*. Zenodo. https://doi.org/10.5281/zenodo.17650994

Randelhoff, A., Fer, I., & Sundfjord, A. (2017). Turbulent upper-ocean mixing affected by meltwater layers during Arctic summer. *Journal of Physical Oceanography*, *47*(4), 835–853. https://doi.org/10.1175/JPO-D-16-0200.1

Rantanen, M., Karpechko, A. Y., Lipponen, A., Nordling, K., Hyvärinen, O., Ruosteenoja, K., et al. (2022). The Arctic has warmed nearly four times faster than the globe since 1979. *Communications Earth & Environment*, *3*(1), 168. https://doi.org/10.1038/s43247-022-00498-3

Ricker, R., Kauker, F., Schweiger, A., Hendricks, S., Zhang, J., & Paul, S. (2021). Evidence for an increasing role of ocean heat in arctic winter sea ice growth. *Journal of Climate*, 1–42. https://doi.org/10.1175/JCLI-D-20-0848.1

Rousset, C., Vancoppenolle, M., Madec, G., Fichefet, T., Flavoni, S., Barthélemy, A., et al. (2015). The Louvain-La-Neuve sea ice model LIM3.6: Global and regional capabilities. *Geoscientific Model Development*, *8*(10), 2991–3005. https://doi.org/10.5194/gmd-8-2991-2015

Serreze, M. C., & Barry, R. G. (2011). Processes and impacts of Arctic amplification: A research synthesis. *Global and Planetary Change*, *77*(1), 85–96. https://doi.org/10.1016/j.gloplacha.2011.03.004

Sicard, M., Kageyama, M., Charbit, S., Braconnot, P., & Madeleine, J.-B. (2022). An energy budget approach to understand the Arctic warming during the last interglacial. *Climate of the Past*, *18*(3), 607–629. https://doi.org/10.5194/cp-18-607-2022

Sime, L. C., Diamond, R., Stepanek, C., Brierley, C., Schroeder, D., Kageyama, M., et al. (2025). A sea ice free arctic: Assessment fast track abrupt-127k experimental protocol and motivation. *EGUsphere*, *2025*, 1–33. https://doi.org/10.5194/egusphere-2025-3531

Sime, L. C., Sivankutty, R., Vallet-Malmierca, I., de Boer, A. M., & Sicard, M. (2023). Summer surface air temperature proxies point to near-sea-ice-free conditions in the Arctic at 127↘ka. *Climate of the Past*, *19*(4), 883–900. https://doi.org/10.5194/cp-19-883-2023

Smith, C. J., Kramer, R. J., Myhre, G., Alterskjær, K., Collins, W., Sima, A., et al. (2020). Effective radiative forcing and adjustments in CMIP6 models. *Atmospheric Chemistry and Physics*, *20*(16), 9591–9618. https://doi.org/10.5194/acp-20-9591-2020

Stroeve, J. C., Markus, T., Boisvert, L., Miller, J., & Barrett, A. (2014). Changes in Arctic melt season and implications for sea ice loss. *Geophysical Research Letters*, *41*(4), 1216–1225. https://doi.org/10.1002/2013GL058951

Sumata, H., de Steur, L., Divine, D. V., Granskog, M. A., & Gerland, S. (2023). Regime shift in Arctic Ocean sea ice thickness. *Nature*, *615*(7952), 443–449. https://doi.org/10.1038/s41586-022-05686-x

Vermassen, F., O'Regan, M., de Boer, A., Schenk, F., Razmjooei, M., West, G., et al. (2023). A seasonally ice-free Arctic Ocean during the Last Interglacial. *Nature Geoscience*, *16*(8), 723–729. https://doi.org/10.1038/s41561-023-01227-x

References From the Supporting Information

Boucher, O., Servonnat, J., Albright, A. L., Aumont, O., Balkanski, Y., Bastrikov, V., et al. (2020). Presentation and evaluation of the IPSL-CM6A-LR climate model. *Journal of Advances in Modeling Earth Systems*, *12*(7), e2019MS002010. https://doi.org/10.1029/2019MS002010

Cao, J., Wang, B., Yang, Y.-M., Ma, L., Li, J., Sun, B., et al. (2018). The NUIST Earth System Model (NESM) version 3: Description and preliminary evaluation. *Geoscientific Model Development*, *11*(7), 2975–2993. https://doi.org/10.5194/gmd-11-2975-2018

Danabasoglu, G., Lamarque, J.-F., Bacmeister, J., Bailey, D. A., DuVivier, A. K., Edwards, J., et al. (2020). The community Earth system model version 2 (CESM2). *Journal of Advances in Modeling Earth Systems*, *12*(2), e2019MS001916. https://doi.org/10.1029/2019MS001916

Döscher, R., Acosta, M., Alessandri, A., Anthoni, P., Arsouze, T., Bergman, T., et al. (2022). The EC-Earth3 Earth system model for the coupled model intercomparison project 6. *Geoscientific Model Development*, *15*(7), 2973–3020. https://doi.org/10.5194/gmd-15-2973-2022

Guo, C., Bentsen, M., Bethke, I., Ilicak, M., Tjiputra, J., Toniazzo, T., et al. (2019). Description and evaluation of NorESM1-F: A fast version of the Norwegian Earth system model (NorESM). *Geoscientific Model Development*, *12*(1), 343–362. https://doi.org/10.5194/gmd-12-343-2019

Hajima, T., Watanabe, M., Yamamoto, A., Tatebe, H., Noguchi, M. A., Abe, M., et al. (2020). Development of the MIROC-ES2L Earth system model and the evaluation of biogeochemical processes and feedbacks. *Geoscientific Model Development*, *13*(5), 2197–2244. https://doi.org/10.5194/gmd-13-2197-2020

Kwok, R., & Rothrock, D. A. (2009). Decline in Arctic sea ice thickness from submarine and ICESat records: 1958–2008. *Geophysical Research Letters*, *36*(15), L15501. https://doi.org/10.1029/2009GL039035

Williams, K. D., Copsey, D., Blockley, E. W., Bodas-Salcedo, A., Calvert, D., Comer, R., et al. (2018). The met office global coupled model 3.0 and 3.1 (GC3.0 and GC3.1) configurations. *Journal of Advances in Modeling Earth Systems*, *10*(2), 357–380. https://doi.org/10.1002/2017MS001115

Ziehn, T., Chamberlain, M. A., Law, R. M., Lenton, A., Bodman, R. W., Dix, M., et al. (2020). The Australian Earth system model: ACCESS-ESM1.5. *Journal of Southern Hemisphere Earth Systems Science*, *70*(1), 193–214. https://doi.org/10.1071/ES19035